Hydrothermal Synthesis of Sr-doped Hydroxyapatite and Its Antibacterial Activity

Teodóra Nagyné-Kovács[1*], Boglárka Mészáros[1], Mónika Molnár[2], Mária Tolner[2],
István Endre Lukács[3], Imre M. Szilágyi[1], György Pokol[1,4]

[1] Department of Inorganic and Analytical Chemistry, Faculty of Chemical Technology and Biotechnology,
  Budapest University of Technology and Economics, H-1111 Budapest, Műegyetem rakpart 3., Hungary
[2] Department of Applied Biotechnology and Food Science, Faculty of Chemical Technology and Biotechnology,
  Budapest University of Technology and Economics, H-1111 Budapest, Műegyetem rakpart 3., Hungary
[3] Institute for Technical Physics and Materials Science, Centre for Energy Research, Hungarian Academy of Sciences,
  H-1121 Budapest, Konkoly Thege M. út 29-33, Hungary
[4] Research Centre for Natural Sciences, Hungarian Academy of Sciences, H-1117 Budapest, Magyar tudósok körútja 2., Hungary
* Corresponding author, e-mail: kovacs.teodora@mail.bme.hu

Abstract

In this study, we prepared hydroxyapatite (HAP) samples using hydrothermal method. We investigated the effect of reaction conditions such as phosphate excess applying 1.49 and 1.67 (as stoichiometric) Ca/P ratio, pH (9/ 10/ 11/ 12) and time (4/ 8/ 12/ 24 h). Sample characterization was carried out by XRD and SEM. The results showed, all samples had HAP structure, however, lower Ca/P ratio, larger reaction time and setting the pH to 10 increased the crystallinity. Then, we synthetized Sr-doped HAP samples, varying the Sr concentration using 2, 4, 6, 8 and 10 % Sr/ (Ca+Sr). The Sr content was revealed by EDX. Sr-incorporation did not change the obtained crystalline HAP phase but the unit cell parameters increased. We calculated lattice constants and found that a, b changed from 9.4310 Å to 9.4700 Å, c from 6.8819 Å to 6.9227 Å and the unit cell volume from 530.0951 Å^3 to 537.6556 Å^3 due to the larger ionic radius of Sr compared to Ca. The pure and doped samples had uniform, mostly needle-like morphology with 100-300 nm length and 25-100 nm. In vitro cytotoxicity tests revealed evident antibacterial activity in the case of doped samples compared to pure HAP against *E. coli*.

Keywords

Sr-doped hydroxyapatite, hydrothermal, nanoparticles, lattice parameters, antibacterial activity

1 Introduction

Hydroxyapatite (HAP, $Ca_{10}(PO_4)_6OH_2$) has become one of the most investigated biomaterials over the past few decades due to its excellent biocompatibility and bonding ability to natural tissues. In nature it can be found among the components of hard tissues such as bone, enamel and dentine. In its natural form the molar ratio of Ca/ P is less than the stoichiometric 1.67 due to the presence of significant amounts of CO_3^{2-}, HPO_4^{2-}, Na^+ and Mg^{2+} ions and various trace elements such as Sr^{2+}, Zn^{2+}, Fe^{2+}, F^- [1–7]. Since the chemical formula and physico-chemical properties of the synthetic HAP are so similar to those in the living tissues, it is suitable for many medical applications. It can be used for bone regeneration and substitution as bone filler, scaffold or implant coating, moreover, it has promising results in drug delivery and releasing systems as well [1, 8, 9].

For promoting its possible applicability in living body, its rejection after implantation should be avoided. To facilitate its integration, synthetic HAP not only has to be biocompatible but should also exhibit antibacterial properties for inhibition of bacterial infections. The development of these characteristics is of great interest and can be achieved by composite formation, loading with drugs or organic components, and metal ion doping [10–13].

During metal ion incorporations mainly Ca^{2+} is replaced by Mg^{2+}, Zn^{2+}, Sr^{2+} and Ag^+. With the usage of Ag the antibacterial activity and non-cytotoxicity increase significantly [9, 14, 15], Mg, Zn and Sr can induce greater osteoconductivity, cytotoxibility or even antimicrobial effect, but Sr can also promote sustained drug release [13, 16–23]. The replacement of Ca^{2+} by another ion modifies the crystal structure by causing unit cell contraction or

expansion depending on the ionic radii, but also has influence on the crystallinity, crystallite size, morphology, surface charge and solubility.

In this study, we prepared pure and Sr-doped HAPs by a simple one-step hydrothermal method. We investigated the effect of Ca/P ratio fixing it at two various values (1.49, 1.67), studied the role of reaction time (4/ 8/ 12/ 24 h) and solution pH (9/ 10/ 11/ 12) on the crystalline structure and morphology of the as-prepared samples. For Sr doping we applied different Sr/ (Ca+Sr) molar ratios namely (2/ 4/ 6/ 8/ 10 %). We analyzed the crystalline phases and morphology of the samples by X-ray powder diffraction (XRD) and scanning electron microscopy (SEM), respectively. In the case of doped samples we applied also energy dispersive X-ray spectroscopy (EDX) for elemental analysis. The efficient ion substitution process generates changes in the crystal structure compared to undoped HAP as Sr^{2+} has larger ionic radius (1.12 Å) than Ca^{2+} (0.99Å). Therefore, the lattice parameters and unit cell volume of the synthetized products were determined as well.

Finally, we tested the antimicrobial properties of the Sr-doped HAPs namely in vitro cytotoxicity by colorimetric reduction of INT (2-(4-Iodophenyl)-3-(4-nitrophenyl)-5-phenyl-2H-tetrazolium chloride) against *Escherichia coli* bacterium strain.

2 Experimental
2.1 Preparation of pure and Sr-doped HAP
For the hydrothermal procedures calcium nitrate tetrahydrate [$Ca(NO_3)_2 \cdot 4H_2O$, Sigma Aldrich] and diammonium hydrogen phosphate [$(NH_4)_2HPO_4$, Sigma Aldrich] were dissolved in 50 ml ion exchanged water separately. After some

minutes of stirring, 15 ml from the solutions were taken out and mixed together in a Teflon-lined autoclave (45 ml acid digestion vessel, Parr Ins.) which was followed by immediate white precipitate formation. Then we adjusted the pH by NH_4OH (25 %, Molar Chemicals). For each hydrothermal treatment 180 °C was applied. Finally, the products were filtered and washed several times with ion exchanged water and ethanol and then dried at 60 °C for 2 hours.

We investigated the role of phosphate excess using a lower Ca/P molar ratio (1.49) besides the stoichiometric value (1.67, **HAP1-2**). Then, we studied the effect of solution pH and reaction time applying 9, 10, 11 and 12 pH (**HAP2-5**) and 4, 8, 12 and 24 h (**HAP2**, **HAP6-8**), respectively, using Ca/P = 1.49 (Table 1).

In the case of Sr-doped HAP samples, specified amount of strontium nitrate [$Sr(NO_3)_2$, (Sigma Aldrich)] was added beside $Ca(NO_3)_2$ and then they were dissolved together. We used Sr in various Sr/(Ca+Sr) molar ratios (2/ 4/ 6/ 8/ 10 %, **SrHAP2-10**, Table 2). All the following reaction steps were the same as in the case of the above detailed synthesis.

2.2 Characterization
For XRD measurements a PANanalytical X'Pert Pro MPD diffractometer with Cu Kα radiation (λ = 0.15418 nm) was applied. For analyzing the morphology of **HAP2-8** a JEOL JSM 5500-LV, for **HAP1** and Sr-doped samples (**SrHAP2-10**) a LEO 1540 XB electron microscope and for EDX measurements a JEOL JSM 5500-LV instrument were used. Lattice parameters were determined by least square refinements using the peak positions of the most intensive reflections [24].

Table 1 Preparation details the hydrothermally treated HAP samples

	HAP1	HAP2	HAP3	HAP4	HAP5	HAP6	HAP7	HAP8
$Ca(NO_3)_2 \cdot 4H_2O$ (M)	1.00	1.00	1.00	1.00	1.00	1.00	1.00	1.00
$(NH_4)_2HPO_4$ (M)	0.60	0.67	0.67	0.67	0.67	0.67	0.67	0.60
Ca/P	1.67	1.49	1.49	1.49	1.49	1.49	1.49	1.49
time (h)	24	24	24	24	24	4	8	12
pH	11	11	9	10	12	10	10	10

Table 2 Preparation details the pure and Sr-doped HAP samples

	SrHAP2	SrHAP4	SrHAP6	SrHAP8	SrHAP10
$Ca(NO_3)_2 \cdot 4H_2O$ (M)	0.98	0.96	0.94	0.92	0.90
$(NH_4)_2HPO_4$ (M)	0.60	0.60	0.60	0.60	0.60
$Sr(NO_3)_2$ (M)	0.02	0.04	0.06	0.08	0.10
Sr/ (Ca+Sr) (mol%)	2	4	6	8	10

2.3 Antimicrobial test

For revealing the antimicrobial properties, i.e. the cyto-toxicity of the pure and Sr-doped HAP samples, we studied their effects on the cell viability of *Escherichia coli* (ATCC 25922) by tetrazolium reduction assay. The tetrazolium/formazan couple is a special redox system acting as proton acceptor or oxidant [25]. In the presence of bacteria, the tetrazolium salt (such as 2-(p-iodophenyl)-3(p-nitrophenyl)-5-phenyl tetrazolium chloride (INT)) is reduced to red formazan which is directly proportional to the viable active cells. Therefore, the test method is considered as a comparatively fast method for evaluating the antibacterial activity of antimicrobial agents.

The tests were carried out using direct contact method in shaken tubes filled with 10 ml Luria-Bertani Broth inoculated with 100-100 µL overnight *E. coli* suspension. **HAP1** and **SrHAP2-10** containing solutions were prepared with the concentration of 3 mg/ml in 3-3 parallels. After 24 and 48 h incubation time we took 200 µL of each sample and pipetted it into the wells of a microtiter plate.

30 µL of sterile INT solution was then added to the cells and the quantity of formazan was measured by recording changes in absorbance at 490 nm by a DIALAB ELx800 microplate reader. All treatments were performed in five replicates. One-way analysis of variance (ANOVA) was performed and all *p* values less than 0.05 were considered statistically significant. To compare the treatments Fisher's least significant difference test was carried out.

3 Results and discussion
3.1 Effect of Ca/P ratio

With the utilization of different Ca/P ratios we examined the effect on the crystalline phases and crystallinity of the products. Based on the XRD patterns both **HAP1** (Ca/P = 1.67) and **HAP2** (Ca/P = 1.49) samples were identified as pure HAP (ICDD 04-016-2958). Comparing their XRD patterns, we concluded that the P excess (lower Ca/P ratio) results improved crystallinity since **HAP2** has sharper and narrower reflections (Fig. 1). Considering this result for investigating the role of applied pH and time we fixed the Ca/P at 1.49.

3.2 Effect of pH

All of the samples prepared at different pH values (9/ 10/ 11/ 12) were pure HAP without any impurities (Fig. 2). According to the XRD patterns, pH does not have any role on the obtained crystalline phases of the products, however,
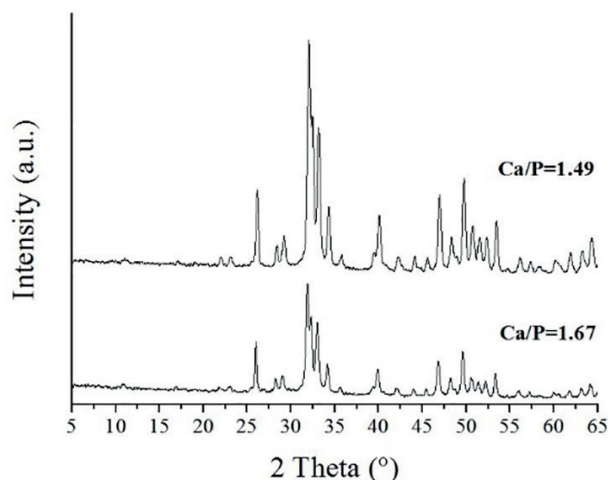

Fig. 1 HAP samples prepared using different Ca/P ratios
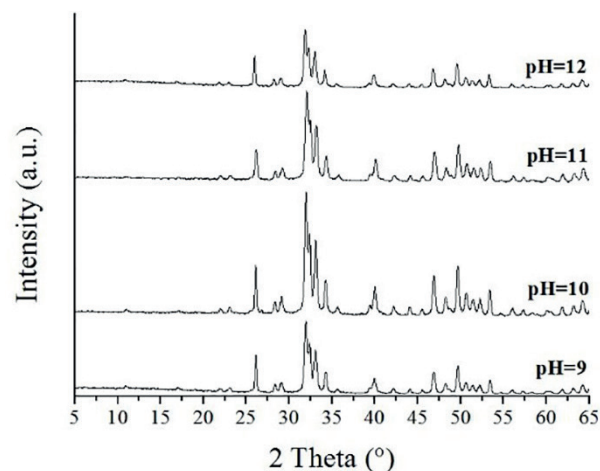(180 °C, 24 h, pH = 11)

Fig. 2 XRD patterns of HAP samples prepared at different pH values
(180 °C, 24 h, Ca/P = 1.49)

it can influence the crystallinity. Increasing the pH from 9 to 10 had favorable effect on the crystallization, however its further rising leads to lower crystallinity. As pH 10 induced the best crystallized samples compared to the others, we applied this value for studying the effect of reaction time.

According to the SEM images, samples prepared at pH 9 and 10 have mainly uniform morphology constituting of longer, needle-like shapes (Fig. 3). Most of the needles have 5-10 µm length and less than 1 µm width. At higher pH much shorter (1-5 µm), elongated crystals formed which were greatly agglomerated. Based on these images, for a well-defined morphology, the lower pH is more beneficial which is in good accordance with the results of the XRD measurements regarding the crystallinity of the samples.
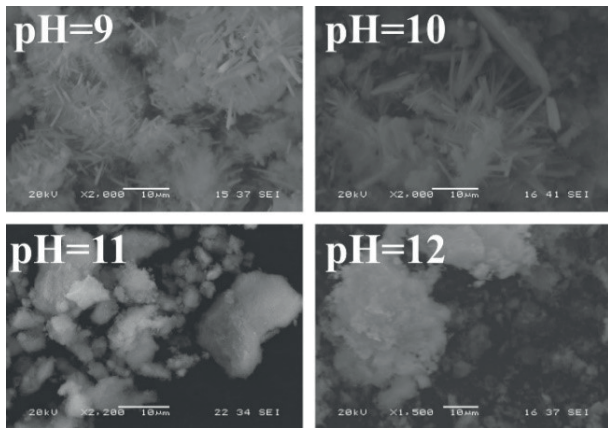
Fig. 3 SEM images of HAP samples prepared at different pH values
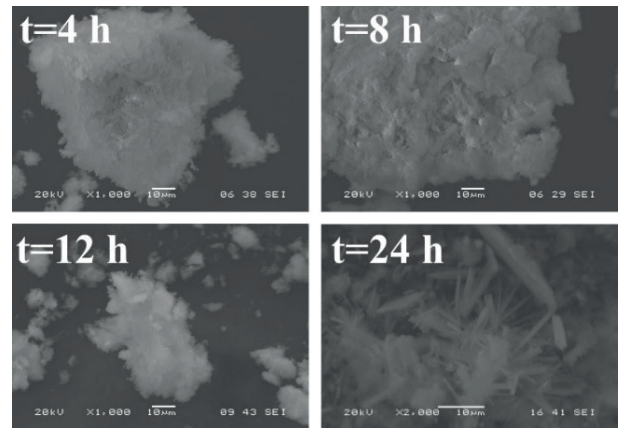(180 °C, 24 h, Ca/P = 1.49)

Fig. 5 SEM images of HAP samples prepared at different time
(180 °C, pH = 10, Ca/P = 1.49)

3.3 Effect of reaction time

For examining the role of reaction time we applied 4/ 8/ 12 and 24 h at 180 °C and pH 10. All XRD peaks were attributed to pure HAP phase in the case of every sample (Fig. 4). Although each sample had the same phase, their crystallinity increased with the employed time: the best crystallized phase was formed at 24 h, as it contains the most intensive and narrowest reflections.

This is also confirmed by the SEM images (Fig. 5) which show that the longer reaction time facilitates the improvement of morphology. During 12 h or less time many short, elongated shapes can be observed mainly on the surface of bigger particles with various sizes. Observably, there are no significant differences in the length or even width of the particles, however it changes greatly with 24 h reaction time. Instead of the initial elongated forms much longer (5-10 μm) and mostly individual rods are obtained.
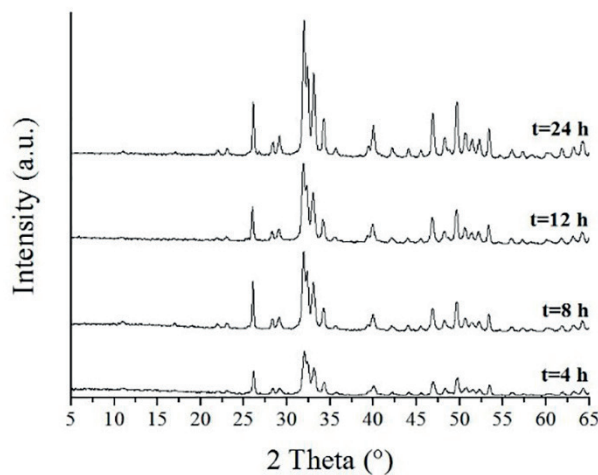
3.4 Sr-doped HAPs

Sr doped samples were synthetized with various Sr amounts (2/ 4/ 6/ 8/ 10 %) at pH 11, 180 °C, 24 h. For comparison the Sr-doped samples to pure HAP we used **HAP1** as reference. All of the reflections of **SrHAP2-10** were attributed to crystalline HAP phase (ICDD 04-016-2958, Fig. 6). The samples were well crystallized consisting of only narrow, sharp peaks without any other Sr-containing or amorphous phase.

The calculated lattice parameters and unit cell volume of the samples are in good accordance with the values found in the reference card (ICDD 04-016-2958, Table 3). The lattice constants of the hexagonal lattice increased due to the larger Sr^{2+} radius (1.12 Å) compared to Ca^{2+} (0.99 Å). Parameter a, b change from 9.4310 Å to 9.4700 Å, c from 6.8819 Å to 6.9227 Å while the unit cell expands from 530.0951 Å^3 to 537.6556 Å^3.

Fig. 4 XRD patterns of HAP samples prepared at different time
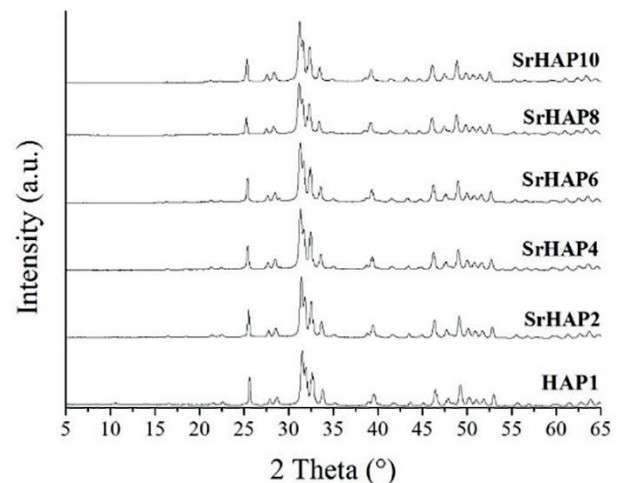(180 °C, pH = 10, Ca/P = 1.49)

Fig. 6 XRD patterns of pure and Sr-doped HAP samples prepared at different time (180 °C, 24 h, pH = 11, Ca/P = 1.67)

Table 3 Calculated lattice parameters of pure and Sr-doped HAP samples

	$a = b$ (Å)	c (Å)	V (Å³)
HAP1	9.4310	6.8819	530.0951
SrHAP2	9.4424	6.8928	532.2157
SrHAP4	9.4488	6.9017	533.6267
SrHAP6	9.4503	6.9063	534.1561
SrHAP8	9.4660	6.9159	536.6787
SrHAP10	9.4700	6.9227	537.6556

Table 4 EDX results of pure and Sr-doped HAP samples

	O atom %	P atom %	Ca atom %	Sr atom %
HAP1	59.7	15.4	24.9	-
SrHAP2	60.8	14.8	23.9	0.5
SrHAP4	61.8	14.5	22.8	0.9
SrHAP6	62.722	14.163	22.113	1.002
SrHAP8	64.306	13.874	20.395	1.424
SrHAP10	65.022	13.853	19.481	1.644

The morphology of the **HAP1**, **SrHAP2** and **SrHAP4** is well defined and homogenous (Fig. 7). These samples consist of ca. 100-150 nm long needles with 25-35 nm width in **HAP1** and **SrHAP2** and with 50 nm at **SrHAP4**. In the case of **SrHAP6** both band-like and needle-like shapes are observed. The ribbons are ca. 100 nm wide and 200-300 nm long while the needles have less than 50 nm width and 100 nm length. Increasing Sr amount, however, facilitates the formation of needles causing uniform morphology in **SrHAP8** and **SrHAP10**. **SrHAP8** contains mostly needles with almost the same width and length (less than 50 nm) but they become bigger, namely 50-100 nm in width and 100-200 nm in length in **SrHAP10**.

To study the elemental composition of the Sr-doped samples and confirm the presence of Sr, EDX was also carried out (Table 4). The main components of the samples were O, P, Ca, while Sr also could be detected in Sr-doped samples with increasing tendency.
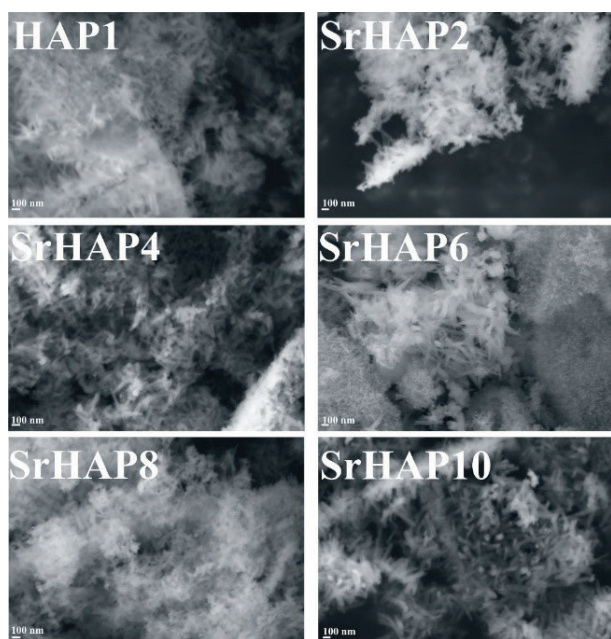

Fig. 7 SEM images of pure and Sr-doped HAP samples
(180 °C, 24 h, pH = 11, Ca/P = 1.67)

3.5 Antibacterial test

For developing the *in vitro* cytotoxic effect of the pure and Sr-doped HAP samples, we performed INT reduction assay.

According to Fig. 8 every sample has obvious inhibiting effect on the cell viability against *E. coli* after both 24 and 48 h incubation time compared to **HAP1.** The higher absorbance means the greater number of viable bacteria. The strongest effect after 24 h belongs to **SrHAP10** (~25 % inhibition compared to pure **HAP)** and even the tendency in the antibacterial activity along with increasing amount of Sr is observable (except **SrHAP6**). Statistically significant decrease (> 20 % inhibition) was found in the case of **SrHAP2, SrHAP8** and **SrHAP10** samples compared to pure **HAP** (Fig. 8) in the case of 48 h exposure time. However, **SrHAP2** also presents as high antibacterial activity as **SrHAP10**. It is also seen, that **SrHAP6** least suits the trend neither at 24 h nor at 48 h incubation time. Since the release of metal ion from the HAP structure has important role in the bactericidal effects among others, it is assumed that in the case of **SrHAP6** it was not enough sufficient.

The results of this study agree with previous observations reported by Ravi et al. [18]. They also reported slight inhibition of Sr-substituted hydroxyapatite applied at 5 and 10 % for *E. coli*.

4 Conclusion

We synthetized pure HAP samples by simple, one-step hydrothermal method. We examined the role of different Ca/P ratios, pH and time on the crystalline phases and the morphology as well. All the prepared samples were pure crystalline HAP, the changed parameters did not have effect the obtained crystalline phase. We found that lower, i.e. 1.49 Ca/P ratio resulted better-crystallized phase compared to the stoichiometric 1.67 ratio. 9/ 10/ 11 and 12 pH values were used and pH 10 was considered to improve the crystallinity the greatest. The SEM images showed that at pH 9, 10 mostly uniform, needle-like shapes with 5-10 μm
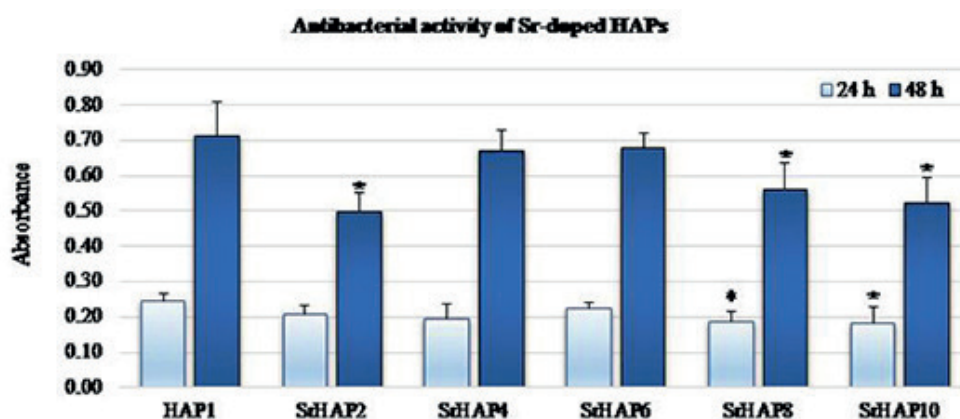
Fig. 8 Tetrazolium reduction results for Sr-doped HAPs (Asterisks indicate significant difference from the HAP1 (level of significance: $p < 0.05$)

length and less than 1 μm width formed, while shorter (1-5 μm) needles grew at 11 and 12 pH. Increasing reaction time from 4 to 8, 12 and 24 h enhanced the crystallinity of the samples, however, their morphology changed remarkably only after 12 h. Till that time only short, elongated shapes greatly stuck to each other formed while at 24 h these shapes became longer (5-10 μm), individual needles. Sr-doped samples were identified also as HAP structures, although, the presence of Sr was detected by EDX in the case of all samples. The lattice constants *a, b* changed from 9.4310 Å to 9.4700 Å, *c* from 6.8819 Å to 6.9227 Å and the volume from 530.0951 Å³ to 537.6556Å³ due to the larger ionic radius of Sr compared to Ca. Every sample had mostly uniform morphology which changed a bit along with the greater amount of Sr. **HAP1** and **SrHAP2** constituted of 100-150 nm long needles with 25-35 nm width so did **SrHAP4** but with 50 nm width. In the case of **SrHAP6** both 100 nm wide, 200-300 nm long bands and less than 50 nm wide and 100 nm long needles formed. **SrHAP8** and **SrHAP10** composed of needles which were less than 50 nm long and wide but 50-100 nm in width and 100-200 nm, respectively. *In vitro* cytotoxicity tests revealed obvious effective bactericidal properties in the case of doped

samples compared to pure HAP against *E. coli*. Trend in decreasing absorbance due to the increasing amount of Sr was also observable in most cases.

Acknowledgments

References

[1] Szcześ, A., Hołysz, L., Chibowski, E. "Synthesis of Hydroxyapatite for Biomedical Applications", Advances in Colloid and Interface Science, 249, pp. 321–330, 2017.
https://doi.org/10.1016/j.cis.2017.04.007

[2] Sadat-Shojai, M., Khorasani, M.-T., Dinpanah-Khoshdargi, E., Jamshidi, A. "Synthesis Methods for Nanosized Hydroxyapatite with Diverse Structures", Acta Biomaterialia, 9(8), pp. 7591–7621, 2013.
https://doi.org/10.1016/j.actbio.2013.04.012

[3] Combes, C., Cazalbou, S., Rey, C. "Apatite Biominerals", Minerals, 6(2), article ID: 34, 2016.
https://doi.org/10.3390/min6020034

[4] Florencio-Silva, R., da Silva Sasso, G. R., Sasso-Cerri, E., Simões, M. J., Cerri, P. S. "Biology of Bone Tissue: Structure, Function, and Factors That Influence Bone Cells", BioMed Research International, 2015, article ID: 421746, 2015.
https://doi.org/10.1155/2015/421746

[5] Ratnayake, J. T. B., Mucalo, M., Dias, G. J. "Substituted Hydroxyapatites for Bone Regeneration: A Review of Current Trends", Journal of Biomedical Materials Research: Part B Applied Biomaterials, 105(5), pp. 1285–1299, 2017.
https://doi.org/10.1002/jbm.b.33651

[6] Šupová, M. "Substituted Hydroxyapatites for Biomedical Applications: A Review", Ceramics International, 41(8), pp. 9203–9231, 2015.
https://doi.org/10.1016/j.ceramint.2015.03.316

[7] Downey, P. A., Siegel, M. I. "Bone Biology and the Clinical Implications for Osteoporosis", Physical Therapy, 86(1), pp. 77–91, 2006.
https://doi.org/10.1093/ptj/86.1.77

[8] Suganthi, R. V., Elayaraja, K., Joshy, M. I. A., Chandra, V. S., Girija, E. K., Kalkura, S. N. "Fibrous Growth of Strontium Substituted Hydroxyapatite and Its Drug Release", Materials Science and Engineering: C, 31(3), pp. 593–599, 2001.
https://doi.org/10.1016/j.msec.2010.11.025

[9] Xie, C.-M., Lu, X., Wang, K.-F., Meng, F.-Z., Jiang, O., Zhang, H.-P., Zhi, W., Fang, L.-M. "Silver Nanoparticles and Growth Factors Incorporated Hydroxyapatite Coatings on Metallic Implant Surfaces for Enhancement of Osteoinductivity and Antibacterial Properties", ACS Applied Materials and Interfaces, 6(11), pp. 8580–8589, 2014.
https://doi.org/10.1021/am501428e

[10] Chen, L., Hu, J., Ran, J., Shen, X., Tong, H. "Synthesis and Cytocompatibility of Collagen/Hydroxyapatite Nanocomposite Scaffold for Bone Tissue Engineering", Polymer Composites, 37(1), pp. 81–90, 2016.
https://doi.org/10.1002/pc.23157

[11] Gonçalves, E. M., Oliveira, F. J., Silva, R. F., Neto, M. A., Fernandes, M. H., Amaral, M., Vallet-Regí, M., Vila, M. "Three-Dimensional Printed PCL-Hydroxyapatite Scaffolds Filled with CNTs for Bone Cell Growth Stimulation", Journal of Biomedical Materials Research: Part B Applied Biomaterials, 104(6), pp. 1210–1219, 2016.
https://doi.org/10.1002/jbm.b.33432

[12] Kulanthaivel, S., Mishra, U., Agarwal, T., Giri, S., Pal, K., Pramanik, K., Banerjee, I. "Improving the Osteogenic and Angiogenic Properties of Synthetic Hydroxyapatite by Dual Doping of Bivalent Cobalt and Magnesium Ion", Ceramics International, 41(9), pp. 11323–11333, 2015.
https://doi.org/10.1016/j.ceramint.2015.05.090

[13] Hao, Y., Yan, H., Wang, X., Zhu, B., Ning, C., Ge, S. "Evaluation of Osteoinduction and Proliferation on Nano-Sr-HAP: A Novel Orthopedic Biomaterial for Bone Tissue Regeneration", Journal of Nanoscience and Nanotechnology, 12(1), pp. 207–212, 2012.
https://doi.org/10.1166/jnn.2012.5125

[14] Shi, C., Gao, J., Wang, M., Fu, J., Wang, D., Zhu, Y. "Ultra-Trace Silver-Doped Hydroxyapatite with Non-Cytotoxicity and Effective Antibacterial Activity", Materials Science and Engineering: C, 55, pp. 497–505, 2015.
https://doi.org/10.1016/j.msec.2015.05.078

[15] Nagyné-Kovács, T., Studnicka, L., Kincses, A., Spengler, G., Molnár, M., Tolner, M., Lukács, I. E., Szilágyi, I. M., Pokol, G. "Synthesis and Characterization of Sr and Mg-Doped Hydroxyapatite by a Simple Precipitation Method", Ceramics International, 44(18), pp. 22976–22982, 2018.
https://doi.org/10.1016/j.ceramint.2018.09.096

[16] Lin, K., Liu, P., Wei, L., Zou, Z., Zhang, W., Qian, Y., Shen, Y., Chang, J. "Strontium Substituted Hydroxyapatite Porous Microspheres: Surfactant-Free Hydrothermal Synthesis, Enhanced Biological Response and Sustained Drug Release", Chemical Engineering Journal, 222, pp. 49–59, 2013.
https://doi.org/10.1016/j.cej.2013.02.037

[17] Raucci, M. G., Giugliano, D., Alvarez-Perez, M. A., Ambrosio, L. "Effects on Growth and Osteogenic Differentiation of Mesenchymal Stem Cells by the Strontium-Added Sol-Gel Hydroxyapatite Gel Materials", Journal of Materials Science: Materials in Medicine, 26, article ID: 90, 2015.
https://doi.org/10.1007/s10856-015-5436-0

[18] Ravi, N. D., Balu, R., Sampath Kumar, T. S. "Strontium-Substituted Calcium Deficient Hydroxyapatite Nanoparticles: Synthesis, Characterization, and Antibacterial Properties", Journal of the American Ceramic Society, 95(9), pp. 2700–2708, 2012.
https://doi.org/10.1111/j.1551-2916.2012.05262.x

[19] Geng, Z., Cui, Z., Li, Z., Zhu, S., Liang, Y., Liu, Y., Li, X., He, X., Yu, X., Wang, R., Yang, X. "Strontium Incorporation to Optimize the Antibacterial and Biological Characteristics of Silver-Substituted Hydroxyapatite Coating", Materials Science and Engineering: C, 58, pp. 467–477, 2016.
https://doi.org/10.1016/j.msec.2015.08.061

[20] Landi, E., Logroscino, G., Proietti, L., Tampieri, A., Sandri, M., Sprio, S. "Biomimetic Mg-Substituted Hydroxyapatite: From Synthesis to in Vivo Behaviour", Journal of Materials Science: Materials in Medicine, 19(1), pp. 239–247, 2008.
https://doi.org/10.1007/s10856-006-0032-y

[21] Webster, T. J., Ergun, C., Doremus, R. H., Bizios, R. "Hydroxylapatite with Substituted Magnesium, Zinc, Cadmium, and Yttrium. II. Mechanisms of Osteoblast Adhesion", Journal of Biomedical Materials Research, 59, pp. 312–317, 2002.
https://doi.org/10.1002/jbm.1247

[22] Sutha, S., Dhineshbabu, N. R., Prabhu, M., Rajendran, V. "Mg-Doped Hydroxyapatite/Chitosan Composite Coated 316L Stainless Steel Implants for Biomedical Applications", Journal of Nanoscience and Nanotechnology, 15(6), pp. 4178–4187, 2015.
https://doi.org/10.1166/jnn.2015.9753

[23] Ghorbani, F. M., Kaffashi, B., Shokrollahi, P., Seyedjafari, E., Ardeshirylajimi, A. "PCL/Chitosan/Zn-Doped NHA Electrospun Nanocomposite Scaffold Promotes Adipose Derived Stem Cells Adhesion and Proliferation", Carbohydrate Polymers, 118, pp. 133–142, 2015.
https://doi.org/10.1016/j.carbpol.2014.10.071

[24] Holland, T. J. B., Redfern, S. A. T. "Unit Cell Refinement from Powder Diffraction Data: The Use of Regression Diagnostics", Mineralogical Magazine, 61(404), pp. 65–77, 1997.
https://doi.org/10.1180/minmag.1997.061.404.07

[25] Moussa, S. H., Tayel, A. A., Al-Hassan, A. A., Farouk, A. "Tetrazolium/Formazan Test as an Efficient Method to Determine Fungal Chitosan Antimicrobial Activity", Journal of Mycology, 2013, article ID: 753692, 2013.
https://doi.org/10.1155/2013/753692